Phase stability and oxygen-sensitive photoluminescence of ZrO_2:Eu,Nb nanopowders

Valter Kiisk [a, *], Laurits Puust [a], Hugo Mandar€ [a], Peeter Ritslaid [a], Mihkel Rahn€ [a], Ivita Bite [b], Dzidra Jankovica [c], Ilmo Sildos [a], Raivo Jaaniso [a]

[a] Institute of Physics, University of Tartu, W. Ostwaldi St 1, 50411 Tartu, Estonia

[b] Institute of Solid State Physics, University of Latvia, Kengaraga St 8, Riga LV-1063, Latvia

[c] Institute of Inorganic Chemistry, Riga Technical University, Miera 34, Salaspils LV-2169, Latvia

highlights

- Charge compensation of $Eu^{3þ}$ ions in ZrO_2 by $Nb^{5þ}$ ions is proposed.
- Simultaneous doping with $Eu^{3þ}$ and $Nb^{5þ}$ ions suppresses the formation of tetragonal ZrO_2.
- Suitable Nb co-doping causes an improvement of $Eu^{3þ}$ luminescence properties.
- Several types of oxygen sensitivity of the $Eu^{3þ}$ luminescence is observed.

abstract

We studied structure and oxygen-sensitive photoluminescence (PL) of ZrO_2:Eu,Nb nanocrystalline powders synthesized via a sol-gel route and heat-treated up to 1200 C. The material containing only 2 at % $Eu^{3þ}$ was predominantly monoclinic, whereas 8 at% of $Eu^{3þ}$ stabilized tetragonal phase. Comparable amount of niobium co-doping effectively suppressed the formation of tetragonal phase.

PL of $Eu^{3þ}$ ions was observed under direct excitation at 395 nm. PL decay kinetics showed that the luminescence was partially quenched, depending on doping concentrations and ambient atmosphere. At 300 C, the PL intensity of all samples systematically responded (with up to 70% change) to changing oxygen content in the O_2/N_2 mixture at atmospheric pressure. At low doping levels, the dominant factor controlling the PL intensity was an energy transfer from excited PL centers to randomly distributed defects in the ZrO_2 lattice. We argue that the charge transfer between the defects and adsorbed oxygen molecules alters the ability of the defects to quench $Eu^{3þ}$ luminescence. At high doping levels, another type of sensor response was observed, where some $Eu^{3þ}$ emitters are effectively switched on or off by the change of ambient gas. A remarkable feature of the studied material is a reversing of the sensor response with the variation of the Nb concentration.

1. Introduction

Development of nanophosphors has been a popular topic for a few decades. It is stimulated by special applications (such as bio-imaging [1]), optimization of display and lighting technologies [2] as well as by promising nanoscale mechanisms of luminescence control (quantum confinement, plasmonics, etc). The large surface area to volume ratio also suggests chemical sensing possibilities. Versatility of sensing mechanisms is urgently needed because chemical sensing applications require optimization of numerous parameters (sensitivity, selectivity, stability, power consumption, size, etc). Recent developments show that inorganic luminescent nanoparticles (from quantum dots to various doped nanocrystals) provide a versatile arena for implementing novel materials and methods for optical gas sensing.

Adsorption of different gases on the surfaces of metal oxides has been extensively studied. For example, it was demonstrated quite long ago that even at elevated temperatures (400 C) oxygen pickup by ZrO_2, occurring over timescales of 10^2e10^3 s, is

predominately a surface phenomenon [3]. A fraction of oxygen was found to be reversibly adsorbed. It was proposed that the adsorbed oxygen molecule captures an electron from the conduction band and this electron, in turn, originates from an anion vacancy acting as electron donor. This scheme seems to be common for many metal oxides, of which some semiconductors (TiO_2, SnO_2, etc) are also good conductometric gas sensors [4].

This mechanism implies that in sufficiently fine-grained ma-terials most donor sites become ionized when exposed to oxygen. It is possible that majority of optical centers in the material also participate in or are influenced by the charge transfer. The sensor response of luminescence centers is especially interesting as luminescence is a two-step process (excitation and emission), so that external influences have more chances to intercept the photon emission. Such oxygen sensing effect has been recently observed in several trivalent rare earth (RE) activated nano-crystalline matrices: $CePO_4:Tb^{3+}$ [5], TiO_2:Sm [6,7], $ZrO_2:Eu^{3+}$ [8,9], and $Pr:K_{0.5}Na_{0.5}NbO_3$ [11]. In most cases, it is believed that, at certain charge state, the electron donor site becomes lumi-nescence quenching center. Unlike the conventional oxygen probes based on direct quenching of the PL by oxygen molecules [12], this mechanism can cause either increase or decrease of the PL intensity as the material is exposed to oxygen. At least in the case of TiO_2:Sm and ZrO_2:Eu the physics of adsorption and/or luminescence quenching is such that a significant luminescence response is realized already at oxygen concentrations below 1 vol

% [7,9]. Hence, such materials may be promising for trace oxygen sensing, or oxygen sensing over a wide dynamic range. Advan-tages of Eu^{3+} over other RE ions and the intrinsic luminescence centers in ZrO_2 were argued elsewhere [9]. In particular, the emitter can withstand elevated temperatures frequently required for viable sensor operation or industrial setting.

The common stable phase of nominally pure zirconia is the monoclinic one (m-ZrO_2). At sufficiently high temperatures a martensitic transformation first into tetragonal (t-ZrO_2) and then into cubic (c-ZrO_2) polymorph takes place [10]. Due to charge dif-ference (and sometimes also size mismatch), trivalent RE ions do not naturally substitute into MeO_2-type crystalline hosts. Doping with such aliovalent impurities may induce charge compensating defects, such as anion or cation vacancies. It is believed that the structural distortion induced by oxygen vacancies constitutes one of the mechanisms by which the metastable t-ZrO_2 or c-ZrO_2 phases become stable at room temperature [13]. On the other hand, the large amount of defects and the phase stability issues limit the performance and maximum usable concentration of RE ions for luminescence applications. At least in the case of $ZrO_2:Er^{3+}$, it has been reported that niobium (Nb) co-dopant improves the (up-converted) luminescence performance as well as stability of the dominant monoclinic phase [14,21]. It was shown that in ZrO_2:Eu,Nb the niobium was incorporated as Nb^{5+}, at least close to surface [9]. Hence, comparable amount of Nb co-dopant should compensate the charge difference of the RE^{3+} and Zr^{4+} ions. Moreover, the ionic radii of Zr^{4+}, Eu^{3+} and Nb^{5+} are 78, 101 and 69 pm, respectively (due to Shannon [22], for coordination number 7, as in m-ZrO_2). Hence, there is a chance that Nb^{5+} also compensates for the lattice distortion induced by Eu^{3+}.

In this work, a comprehensive study of the structural, lumi-nescence and gas sensing properties of ZrO_2:Eu and ZrO_2:Eu,Nb were carried out. We demonstrate that co-doping with Nb indeed dramatically affects the phase stability, Eu^{3+} luminescence and its oxygen sensing behavior. These dopings presumably affect mainly the defectiveness in the material bulk. Future studies should also address surface treatment to optimize the oxygen chemisorption [23].

2. Experimental details

ZrO_2:Eu and ZrO_2:Eu,Nb gels were synthesized using a sol-gel route based on $ZrCl_4$ (99.9%), Eu_2O_3 (99.99%), Nb_2O_5 (99.5%) and glycine (99.7%) as precursors (all supplied by Sigma-Aldrich), following the procedure described by Smits et al. [14]. The nomi-nal concentrations of Eu and Nb dopants during synthesis were either 2 or 8 at%. One additional sample was prepared where the concentration of Nb was notably higher than that of Eu (Table 1). The dried gels were annealed at 1200 C for 2 h, except for the samples with the high dopant concentration, which were initially annealed at 1000 C and then at 1200 C to observe the effect of annealing temperature. Annealing resulted in white powdered materials.

For structural and chemical characterization of the obtained materials, several techniques were used. X-ray diffraction (XRD) patterns were recorded in BraggeBrentano configuration using Rigaku™ SmartLab diffractometer (Cu Ka radiation, 8.1 kW tube power). Apparent volume weighted size of coherently diffracting domains was calculated (using program AXES) over the first 20 reflections of monoclinic phase or over all reflections of tetragonal phase. LaB_6 (SRM660) was used as reference material for taking into account geometric broadening of diffraction peaks. Concen-tration of crystalline phases was evaluated from XRD Rietveld analysis (program FULLPROF [15]) by taking into account mono-clinic, tetragonal and cubic phases of zirconia and monoclinic europium orthoniobate. Structure data of cubic zirconia were taken from Martin et al. [16] (ICSD collection code 72955) or from Jørgensen et al. [17] (ICSD collection code 62445), monoclinic zir-conia from Wang et al. [18] (ICSD collection code 89426), tetragonal zirconia from Malek et al. [19] (ICSD collection code 85322) and for $Eu_xNbO_{4\ 1.5(1\ x)}$ from Toda et al. [20] (ICSD collection code 92239).

Crystalline phase was additionally confirmed from Raman spectra, acquired with Renishaw inVia micro-spectrometer using 514 nm laser excitation. Impurity content (only in the co-doped samples) was evaluated from X-ray fluorescence (XRF) spectra us-ing Rigaku ZSX 400 spectrometer.

Laser-stimulated PL and its gas response measurements were carried out using a lab-assembled setup, where the powder was fixed by a drop of high-purity methanol on the heating/cooling stage inside a gas-tight chamber with an optical window (Linkam THMS350V). Mass-flow controllers were used to achieve a constant flow (200 cm^3/min) of oxygen/nitrogen mixture through the chamber. The 99.999% purity source gases were used. A 395 nm laser diode (Toptica LD-0395-0120-1) was used for excitation because of its good resonance with the most pronounced 4f–4f excitation peak of Eu^{3+} [24] (see also Supplementary Information).

Table 1
List of sol-gel-prepared zirconia samples used in this study. For co-doped materials, impurity concentrations were determined from X-ray fluorescence measurements. T_a is annealing temperature, C is concentration of crystalline phases other than monoclinic, L is the crystallite size in dominant phase and R_{wp} is conventional Rietveld R-factor (residual error) for the XRD pattern.

Chemical composition (at%)	T_a (C)	C (mass%)	L (nm)	R_{wp}
ZrO_2:Eu(2)	1200	6 ± 2		19
ZrO_2:Eu(2.12)Nb(1.87)	1200	3 ± 1		21
ZrO_2:Eu(1.48)Nb(2.74)	1200	4 ± 1	49 ± 8	17
ZrO_2:Eu(8)	1000	100	15 ± 8	8
	1200	100	25 ± 4	e[a]
ZrO_2:Eu(8.68)Nb(8.12)	1000	30±2	34 ± 12	27
	1200	31±2	35 ± 8	33

[a] Rietveld refinement was not performed. The sample contained only tetragonal phase of zirconia.

The emitted PL was collected in a backscattering geometry, dispersed by a monochromator (LOMO MDR-23) and detected either by a CCD camera (Andor DU240-BU) or a photomultiplier tube (Hamamatsu R2949) with a photon counting multiscaler (Fast ComTec P7888). The same laser diode was also utilized in PL decay kinetics measurements by supplying rectangular current pulses with a duration of 500 ms and repetition rate 100 Hz. The good stability of such pulsed light source allowed comparing more reli-ably the signal strengths of different decay curves. The time reso-lution in PL decay kinetics measurements was 100 ns. Gas sensitivity measurements were always carried out at 300 C, which provided stronger and more stable gas response in the PL, as compared to room temperature [9].

3. Results

Scanning electron microscopy for such kind of material was reported already in a previous work [9], showing overall meso-porous structure and strongly agglomerated particle-like forma-tions with diameters ranging over 200–600 nm. Transmission electron microscopy could distinguish individual particles as small as 100 nm (see Supplementary Information). The results of XRF analysis are in a reasonable agreement with the nominal dopant concentrations used in synthesis (Table 1). Hereafter we analyze more systematically the manifestations of impurity content in the XRD, Raman and PL data.

Phase composition of the samples was evaluated from XRD analysis. In the case of the three samples with 2 at% nominal Eu concentration, all reflections, except one at $2\theta \approx 30.12$, were identified belonging to monoclinic ZrO_2 (Fig. 1). The reflection at 30.12 is a trace of the strongest reflection of tetragonal (or cubic) ZrO_2. The concentration of the tetragonal phase, calculated by Rietveld analysis, is reported in Table 1. The tetragonal phase con-centration is the highest (6 ± 2 mass%) for the sample containing only Eu dopant. Addition of Nb reduces the amount of this trace phase.

The remaining two samples had quite different phase compo-sition (Fig. 1). For the sample containing 8 at% of Eu, all reflections can be indexed as reflections of tetragonal ZrO_2. The broadening of the reflections is considerably larger compared to the other

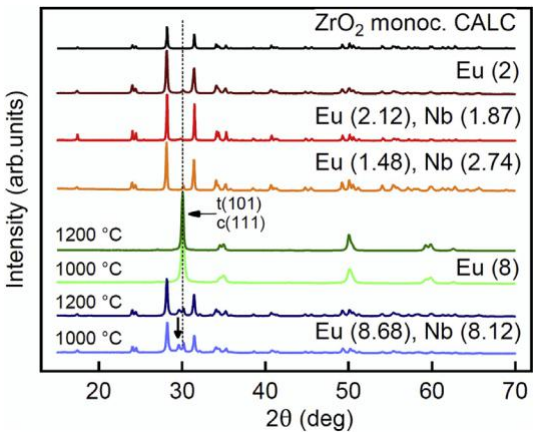

Fig. 1. X-ray diffraction patterns of the sol-gel-derived ZrO_2:Eu and ZrO_2:Eu,Nb pow-ders annealed at 1200 C. The top-most pattern was calculated for monoclinic ZrO_2 (ICSD collection code 89426). Reflection at 30.12 (labeled), not belonging to mono-clinic phase, can be indexed as 101 tetragonal or 111 cubic phase. Vertical arrow pointing at 29.58 marks the position of reflection 111 of cubic $Eu_{0.5}Zr_{0.5}O_{1.75}$ [17]. The XRD patterns of the samples with high impurity content are shown both for 1000 C (light color) and 1200 C (dark color) annealing temperatures.

samples. Annealing at 1200 C retained the pure tetragonal phase but induced notable growth of crystallites (from 15 to 25 nm, see Table 1), as shown by a narrowing of the reflections.

Most reflections of the sample ZrO_2:Eu(8.68),Nb(8.12), annealed at 1000 C, can be indexed as related to monoclinic ZrO_2. Relatively strong reflections at 29.6 and 30.18 can be assigned belonging to cubic $Eu_xZr_{1-x}O_{2-x/2}$ (where $x = 0.5$, ICDD PDF card number 78-1292 or ICSD collection code 62445) and tetragonal (or cubic) ZrO_2, correspondingly. A few remaining weak reflections (e.g. at 32.13 and 47.2) can be assigned to monoclinic $Eu_xNbO_{4-1.5(1-x)}$ (ICSD collection code 92239) and the rest (e.g. at 28.9 and 48.4) to cubic $Eu_6Nb_2O_{14}$ (ICDD PDF card number 26-0633). According to Rietveld analysis the maximal concentration of the trace phases in this sample was 30 mass%. Interestingly, further annealing of this sample at 1200 C did not induce any remarkable growth of crys-tallites or detectable changes in phase composition (Table 1).

The Raman spectra are in full agreement with XRD results (Fig. 2). In the 2 at% Eu-doped sample, one can detect (in addition to the peaks due to monoclinic phase) also two weak Raman peaks at 150 and 260 cm^{-1}, which indicates that the 3–6 mass% of the metastable phase detected by XRD is tetragonal one. The spectrum of ZrO_2:Eu(8%) is completely transformed and represents fully stabilized tetragonal phase; no peaks due to monoclinic (or cubic) zirconia were detected.

The Raman spectrum of ZrO_2:Eu(8.68),Nb(8.12) is very similar to the spectra of the 2 at% samples except for additional weak lines at 230, 415 and 430 cm^{-1}, which may belong to some of the trace phases detected by XRD. It is remarkable that the defectiveness caused by ~17 at% of total impurity concentration and a mixed phase content cannot induce any notable shifting or broadening of the Raman peaks. Similar to XRD results, no changes were detected after annealing at 1200 C.

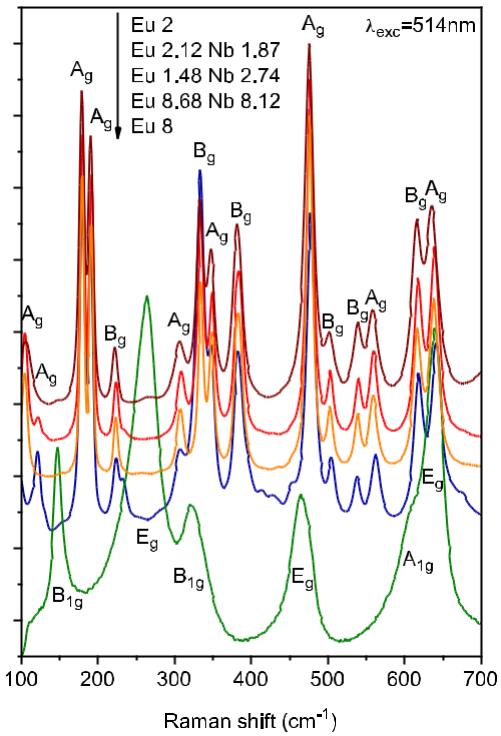

Fig. 2. Raman spectra of the sol-gel-derived ZrO_2:Eu and ZrO_2:Eu,Nb powders annealed at 1200 C. For clarity, the spectra are arbitrarily shifted vertically. In the four topmost spectra, all dominant peaks belong to the monoclinic phase of ZrO_2 [25]. In the last spectrum, all peaks are due to tetragonal phase.

PL emission spectra (under 395 nm excitation) of all annealed powders show typical bands appeared due to $^5D_0/^7F_J$ 4fe4f transitions of trivalent Eu (Fig. 3) [26,27]. Presence of the fine structure shows that all the ^7F_J states are distinctly split by the crystal field, so that $Eu^{3þ}$ emission centers are situated in regular crystalline surrounding. The development of the spectral fine structure across the materials correlates well to the structural data revealed from XRD and Raman measurements. In the three samples with a low Eu concentration as well as for ZrO_2:Eu(8.68)Nb(8.12), the fine structure is characteristic to $Eu^{3þ}$ centers in the monoclinic phase [28e30]. For the sample ZrO_2:Eu(1.48)Nb(2.74), a narrowing of the spectral lines is evident (for instance, the overlapping peaks at 597 nm and 614 nm are better resolved). The spectrum of the 8% Eu doped sample is radically different (Fig. 3) and it is similar to the spectra previously obtained from sol-gel-prepared yttria-stabilized tetragonal zirconia [31]. For both highly doped samples, the minor changes in the PL spectra upon heating at 1200 C are within the experimental variability and may imply a small inhomogeneity of the samples rather than annealing-induced structural changes.

The gas response studies were conducted on all samples at 300 C. The sample was cyclically subjected to pure nitrogen and an oxygen/nitrogen mixture, where the oxygen concentration was precisely controlled between 6 and 100 vol%. Each exposure lasted 10 min while the integrated PL intensity of the strongest $Eu^{3þ}$ emission band was continuously monitored. All samples system-atically responded to the change in oxygen concentration, but the size and sign of the response depended on the sample. In the case of ZrO_2:Eu(2), the PL signal was decreased at increasing oxygen con-centration (Fig. 4). The relative response of the sample ZrO_2:Eu(2.12),Nb(1.87) was much smaller. More interestingly, the

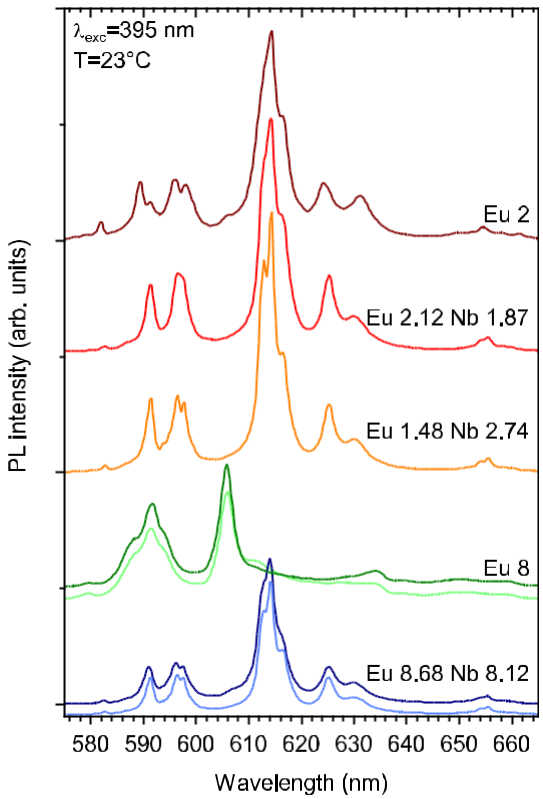

Fig. 3. PL emission spectra of the sol-gel-derived ZrO_2:Eu and ZrO_2:Eu,Nb powders annealed at 1200 C. The spectra are vertically shifted for clarity. The spectra of the samples with high impurity content are shown both for 1000 C (light color) and 1200 C (dark color) annealing temperatures.

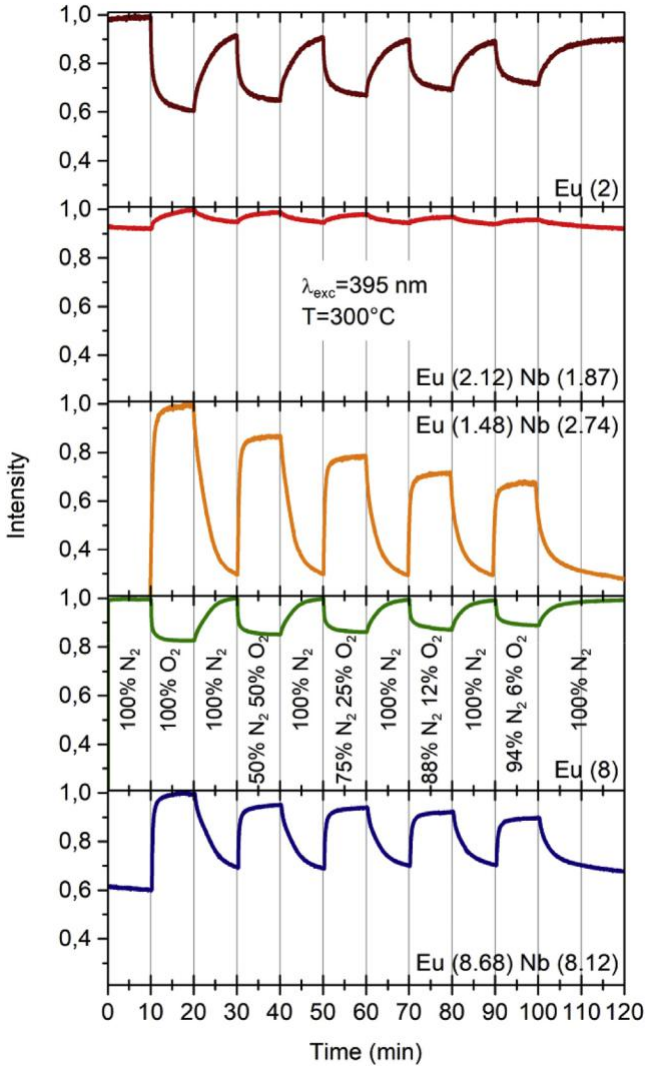

Fig. 4. Temporal behavior of the $Eu^{3þ}$ PL intensity of the ZrO_2:Eu and ZrO_2:Eu,Nb powders (annealed at 1200 C) in response to the ambient oxygen concentration changes at 300 C.

response was reversed. Further increase of Nb concentration (sample ZrO_2:Eu(1.48),Nb(2.74)) resulted in a significant increase of the reversed response. The relative response of this sample (with respect to 100% O_2) is already close to 70% (depending on the relaxation time allowed in nitrogen). Hence, majority of the $Eu^{3þ}$ centers are affected by the gas sensing process. For this material it is also most clearly seen that the response to oxygen is somewhat faster compared to the response to nitrogen. Based on the simple Langmuir adsorption model, such observation is in agreement with the expectation that the primary step of the sensing mechanism is adsorption or desorption of oxygen.

The oxygen response of the tetragonal sample ZrO_2:Eu(8) was very small after annealing at 1000 C (not shown). However, further annealing at 1200 C induced a more definite oxygen sensitivity, with the same type of response as in ZrO_2:Eu(2). Finally, sample ZrO_2:Eu(8.68),Nb(8.12) behaved similarly to ZrO_2:Eu(1.48),Nb(2.74) with somewhat reduced response.

Concerning the stability of the sensor response, it is evident from Fig. 4 that, at the end of each 100% N_2 pulse, the PL signal indeed achieves the same level. Usually such behavior was obtained only during a repeated cycle of gas exposures. Fig. 5 shows an

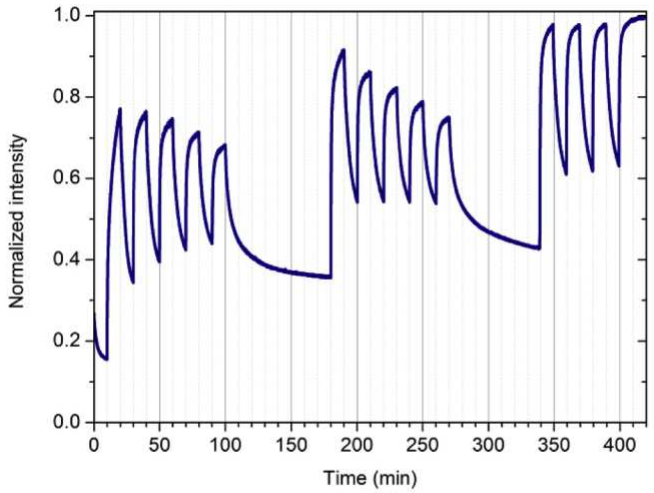

Fig. 5. Behavior of Eu^{3+} PL intensity for the sample ZrO_2:Eu(8.68),Nb(8.12) during three successive cycles of gas exposure. The first two cycles are identical to those in Fig. 4, the last cycle contains alternating exposures to 100% O_2 and 100% N_2 to test for the stability of the response. The signal is arbitrarily normalized and should not be compared to the intensity scale of Fig. 4.

extended measurement. At the beginning, one can recognize certain slow background process with a characteristic time con-stant ~100 min, which affects the absolute PL intensity. The signal becomes stable after 1e2 cycles.

Previous studies have shown that PL decay kinetics is rather informative in revealing essential aspects of the gas sensing mechanism [5e7,9]. The PL decay kinetics was recorded only for the samples that had a significant steady-state oxygen response. For maximum contrast, only decays in 100% O_2 and 100% N_2 were recorded. For all samples, the decay curves were affected by the

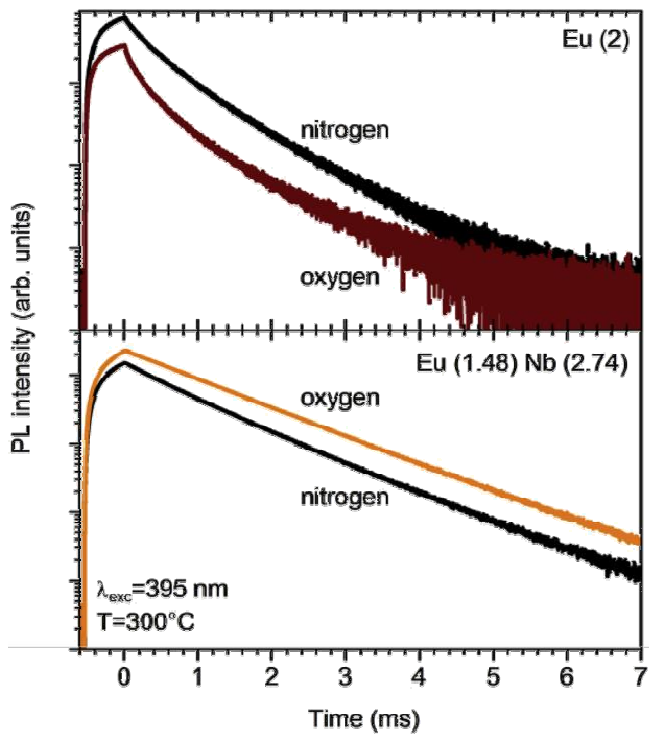

Fig. 6. PL decay kinetics of the ZrO_2:Eu and ZrO_2:Eu,Nb powders (with ~2 at% Eu) in different atmospheres.

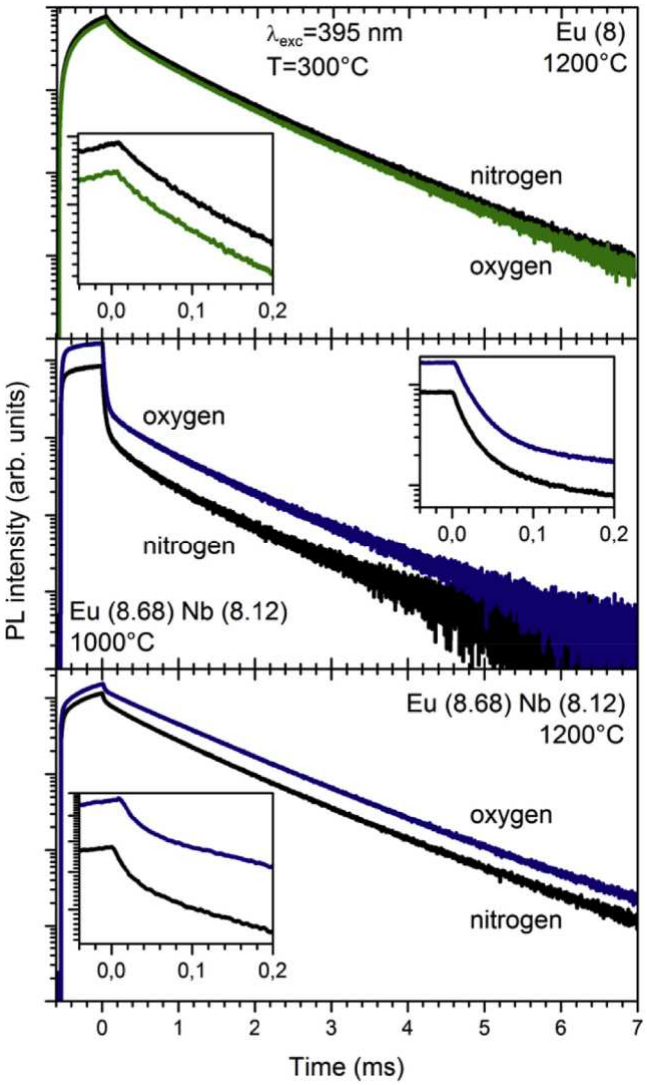

Fig. 7. PL decay kinetics of the ZrO_2:Eu and ZrO_2:Eu,Nb powders (with ~8 at% Eu) in different atmospheres.

ambient atmosphere (Figs. 6 and 7). Their behavior is qualitatively in agreement with Fig. 4. At long time delays from the laser pulse, all PL decays become nearly single exponential with a time constant about 1.1 ms. This represents the natural lifetime of the $^5D_0$ excited state (i.e., radiative decay and possibly some ordered quenching by the immediate surrounding of the Eu^{3+} emitter). Typical reported lifetime of Eu^{3+} emission in m-ZrO_2 and t-ZrO_2 is 1e2 ms [30,31]. It is noteworthy that in the 100% O_2 atmosphere the sample ZrO_2:Eu(1.48),Nb(2.74) had the strongest PL signal as well as nearly perfect single exponential decay (Fig. 6). This must correspond to the state of minimal number of randomly located quenching de-fects in the crystal. Other conditions introduced certain amount of quenching in ZrO_2:Eu(2%) and ZrO_2:Eu(1.48),Nb(2.74), as charac-terized by the gradually decreasing slope of the PL decay profile. Note that the difference between the initial intensities at the beginning of the decay profiles can be attributed to the relatively long excitation pulse (see Appendix).

For the ZrO_2:Eu(8) sample, the slight curvature of the decay curves also implies a small amount of quenching due to energy transfer to randomly located acceptors. However, one cannot recognize any change in the decay profile in the oxygen sensing

experiment. Instead, the decay profile effectively appears to be vertically shifted (Fig. 7), which implies that the number of active Eu^{3+} centers have changed.

The PL decay profile of ZrO_2:Eu(8.68),Nb(8.12) is different and clearly contains two components. Some Eu^{3+} centers experience a strong quenching, as revealed by the fast initial decay (especially for the 1000 C annealing). The rest are regular Eu^{3+} centers exhibiting an exponential PL decay with time constant ~1.1 ms. The contribution of the fast decay is substantially reduced by annealing at 1200 C. At least for the intermediate annealing state, this sample also did not show any notable change of the decay profile as the gas composition was changed.

4. Discussion

The results of structural characterization show that sufficient doping with trivalent europium (about 8 at%) is able to stabilize the material as t-ZrO_2 with no detectable traces of m-ZrO_2 or other phases. The structure is stable against heating to temperatures as high as 1200 C or even more. Such phase purity did not realize when both Eu and Nb dopants were present. Instead, significant reduction in the t-ZrO_2 content was achieved when Eu and Nb concentrations were approximately equal. However, an excess of Nb, as in the sample ZrO_2:Eu(1.48),Nb(2.74), was not efficient to further suppress t-ZrO_2 formation. This is not surprising, because Nb doping alone is also known to stabilize t-ZrO_2 [33]. Hence, complementary pairs of impurity ions can be found (in this case Nb^{5+} and Eu^{3+}) which separately both stabilize t-ZrO_2, but simul-taneous doping with the impurities effectively cancels the stabili-zation. This allows introducing rather high concentration of activators while preserving m-ZrO_2 as the dominant phase.

This was best demonstrated by the highly doped sample ZrO_2:Eu(8.68),Nb(8.12), where Eu^{3+} emission pattern typical to monoclinic surrounding was surprisingly well recovered (Fig. 3), considering the very large (~17 at%) total impurity concentration. However, for lower annealing temperatures, rather strong quenching of luminescence takes place (Fig. 6). Not all Eu^{3+} emit-ters equally experience this PL quenching, as indicated by the rapid initial decay followed by an exponential decay with the regular time constant ~1.1 ms. It is also known that the emission from the Eu^{3+} $^5D_0$ level is not susceptible to cross-relaxation via the long-distance resonant multipolar interaction [34]. The strong PL quenching may characterize specially segregated Eu^{3+} emitters, such as the Eu^{3+} ions situated in the europium-rich phase $Eu_{0.5}Zr_{0.5}O_{1.75}$ detected by XRD analysis. Increased energy migra-tion between such segregated ions can lead to a premature relax-ation of the excitation energy at some defects, and cross-relaxation through non-resonant exchange mechanism can also become relevant [34]. This explanation is compatible with the PL spectra which indicate only Eu^{3+} ions in the monoclinic phase. One can even speculate that the Eu-rich phase effectively separates the grains of monoclinic zirconia. That would explain why annealing at 1200 C did not yield further growth of the monoclinic domains.

Co-doping should induce drastic changes in the vacancy con-centration depending on the Nb^{5+}/Eu^{3+} doping ratio. If an oxygen vacancy occupied a nearest neighbor position of Eu^{3+}, then one would expect a notable change of local symmetry and crystal field strength around the emitter as the vacancy is removed. Interest-ingly, Nb co-doping induced only small changes in the fine struc-ture of Eu^{3+} PL spectrum (Fig. 3). Various studies of yttria-stabilized zirconia have suggested that oxygen vacancy occupies not a nearest neighbor but a next nearest neighbor position which is energeti-cally favored [13]. The assumption is also in agreement with the observation that only single Eu^{3+} site with well-known emission pattern (as in Fig. 3) is commonly identified in the PL spectra of m-ZrO_2:Eu materials. This is the case even in samples prepared by drastically different methods, such as by implantation of Eu^{3+} ions into zirconia films [35].

Although an excess of Nb slightly increased t-ZrO_2 content, the sample ZrO_2:Eu(1.48),Nb(2.74) had the best luminescence and sensor performance: i) a narrowing of the spectral lines is evident (Fig. 3); ii) the PL decay kinetics (in oxygen-containing ambient) is very close to single exponential decay (Fig. 6); iii) strongest oxygen sensing response in the PL intensity is observed (Fig. 4). Tentative scheme explaining these observations is the following. Due to the excess of Nb, only a small amount of oxygen vacancies remains in the material. Hence, the regularity of the crystal lattice is improved leading to a narrowing of the spectral lines. The vacancies are able to hold one or two electrons, forming F-centers. Supposedly, there is certain probability of energy transfer from the excited Eu^{3+} ions to the F-centers resulting in a slight quenching of Eu^{3+} lumines-cence. The acceptors are likely quite randomly distributed leading to a PL decay with gradually decreasing slope (Fig. 6). In an oxygen-rich atmosphere, the adsorbed oxygen molecules capture most of the electrons and ionize nearly all of the remaining vacancies. As a result, the vacancies are not any more capable accepting the energy of excited Eu^{3+} ions and maximum luminescence yield is observed (i.e., single exponential decay with a long lifetime).

Computational quantum mechanical modelling of vacancies in m-HfO_2 (which is structurally almost identical to m-ZrO_2) have predicted optical transitions from middle-gap occupied vacancy states (V^{+}, V^{0} and V) to a resonant state in the conduction band with transition energies about 2.4–2.7 eV and relatively large oscillator strengths [38]. This absorption is spectrally close to the emission transitions of Eu^{3+}. At least for yttria-stabilized zirconia (YSZ), several absorption bands in this region have also been observed experimentally [36,37].

Sample ZrO_2:Eu(2) showed in both 100% O_2 and 100% N_2 a stronger PL quenching compared to ZrO_2:Eu(1.48),Nb(2.74), but the mechanism of quenching (based on the PL decay profile, Fig. 6) looks similar. This is expected owing to the higher amount of ox-ygen vacancies present in ZrO_2:Eu(2) due to uncompensated Eu^{3+} ions. More interestingly, the oxygen response of the PL is reversed. An intermediate case is ZrO_2:Eu(2.12),Nb(1.87), which contained slightly less Nb. The PL of this sample showed only very small ox-ygen sensitivity (Fig. 4). The observations suggest the following explanation. Oxygen vacancies can exist in several charge states. For the sake of discussion, let's suppose that V^{0}, V^{+} and V^{2+} (i.e., oxygen vacancies containing 2, 1 or 0 electrons, respectively) are involved, where only V^{+} occurs to be in a good resonance with Eu $^{3+}$ emission. Upon adsorption of oxygen molecules, certain amount of electrons become trapped at the surface. As a result, some V^{+} centers are converted into V^{2+} whereas some V^{0} centers become V^{+}. Hence, the concentration of V^{+} may either increase or decrease depending on the number of electrons available in the system. In the sample ZrO_2:Eu(2.12),Nb(1.87), the rates of V^{0}/V^{+} and V^{+}/V^{2+} induced by oxygen adsorption happen to be nearly equal so that only a small change of PL intensity is observed. However, it remains to understand the connection of such model to the charge compensation caused by Nb co-doping.

Based on the integrated PL intensity only, the oxygen responses of the samples ZrO_2:Eu(8) and ZrO_2:Eu(8.68),Nb(8.12) could be interpreted in a similar fashion. However, the PL decay profiles of these samples did not show notable changes as the ambient was changed (Fig. 6). The vertical shift of the decay curves rather sug-gests that the number of active Eu^{3+} centers have changed. This might indicate a different kind of reversible redox reaction that can completely switch off the Eu^{3+} center. For instance, the sign of the response of ZrO_2:Eu(8.68),Nb(8.12) conforms to a possibility that Eu^{2+} ions may exist in the material and they are oxidized into

3 þ state when interacting with oxygen. In nitrogen environment, the $Eu^{3þ}$ ions would then reduce back into $Eu^{2þ}$. However, so far, it has not been possible to detect $Eu^{2þ}$ emission in ZrO_2, even when using selective excitation combined with time-resolved spectros-copy [28].

5. Conclusions

Based on the study of sol-gel-prepared crystalline ZrO_2:Eu,Nb nanopowders, we have confirmed that Nb co-dopant has a charge-compensating effect in ZrO_2:Eu. In particular, comparable amount of $Eu^{3þ}$ and $Nb^{5þ}$ dopants strongly suppress formation of t-ZrO_2. At the same time, Nb co-doping only weakly affected the spectral fine structure of $Eu^{3þ}$ luminescence, implying that neither $Nb^{5þ}$ ions nor other charge-compensating defects have direct contact with the $Eu^{3þ}$ ions.

PL decay kinetics showed that certain random defects in the ZrO_2 lattice (possibly oxygen vacancies) partially quench $Eu^{3þ}$ luminescence. A weakly doped material, where $Eu^{3þ}$ was slightly overcompensated by $Nb^{5þ}$, exhibited minimal PL quenching and the best oxygen sensing performance, attributed to a markedly reduced amount of oxygen vacancies. As the main gas sensing mechanism, we propose that adsorbed oxygen molecules capture electrons from the defects and thereby alter their capacity to quench $Eu^{3þ}$ luminescence. Presence of several different types of defects could cause the observed reversing of the sensor response with the variation of dopant content and annealing.

(Fig. A1). The results quite accurately reproduce the PL decays of ZrO_2:Eu(1.48),Nb(2.74). Hence, we can conclude that the difference between the initial intensities at the beginning of the decay profiles of the sample ZrO_2:Eu(1.48),Nb(2.74) (and possibly ZrO_2:Eu(2) as well) can be attributed to the long excitation pulse and does not imply that the number of emitters have changed.

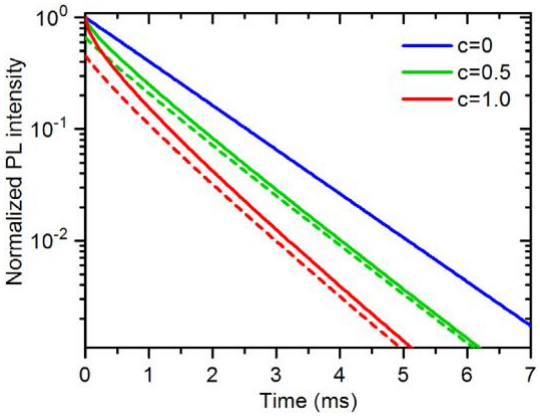

Fig. A1. Simulated PL decay profiles for short excitation pulse (Eqn. (1), solid curves) and long excitation pulse (Eqn. (2), dashed curves). Parameters a ¼ 1=t0 (where t0 ¼ : ¼ pffiffiffiffiffiffi (values of c are indicated on the graph). 1 1 ms) and b c t0

References

[1] P. Reineck, B.C. Gibson, Near-infrared fluorescent nanomaterials for bio-

a

96e98.
[20] K. Toda, M. Honda, Y. Ishimoto, Z.-G. Ye, M. Sato, Oxygen defect in non-stoichiometric europium orthoniobate, $Eu_xNbO_{4-1.5(1-x)}$, Solid State Ionics 136 (2000) 25e30.
[21] K. Smits, D. Olsteins, A. Zolotarjovs, K. Laganovska, D. Millers, R. Ignatans, J. Grabis, Doped zirconia phase and luminescence dependence on the nature of charge compensation, Sci. Rep. 7 (2017) 44453.
[22] R.D. Shannon, Revised effective ionic radii and systematic studies of inter-atomic distances in halides and chalcogenides, Acta Crystallogr. A 32 (1976) 751e767.
[23] V.M. Zhyrovetsky, D.I. Popovych, S.S. Savka, A.S. Serednytski, Nanopowder metal oxide for photoluminescent gas sensing, Nanoscale Res. Lett. 12 (2017) 132.
[24] P. Shi, Z. Xia, M.S. Molokeev, V.V. Atuchin, Crystal chemistry and luminescence properties of red-emitting $CsGd_{1-x}Eux(MoO_4)_2$ solid-solution phosphors, Dalton Trans. 43 (2014) 9669e9676.
[25] P.E. Quintard, P. Barberis, A.P. Mirgorodsky, T. Merle-Mejean, Comparative lattice-dynamical study of the Raman spectra of monoclinic and tetragonal phases of zirconia and hafnia, J. Am. Ceram. Soc. 85 (2002) 1745e1749.
[26] P.A. Tanner, Some misconceptions concerning the electronic spectra of tri-positive europium and cerium, Chem. Soc. Rev. 42 (2003) 5090e5101.
[27] V.V. Atuchin, A.S. Aleksandrovsky, O.D. Chimitova, T.A. Gavrilova, A.S. Krylov, M.S. Molokeev, A.S. Oreshonkov, B.G. Bazarov, J.G. Bazarova, Synthesis and spectroscopic properties of monoclinic a-$Eu_2(MoO_4)_3$, J. Phys. Chem. C 118 (2014) 15404e15411.
[28] K. Smits, L. Grigorjeva, D. Millers, A. Sarakovskis, A. Opalinska, J.D. Fidelus, W. Lojkowski, Europium doped zirconia luminescence, Opt. Mater. 32 (2010) 827e831.
[29] L. Li, H.K. Yang, B.K. Moon, B.C. Choi, J.H. Jeong, K.-W. Jang, H.S. Lee, S.S. Yi, Structure, charge transfer bands and photoluminescence of nanocrystals tetragonal and monoclinic ZrO_2:Eu, J. Nanosci. Nanotechnol. 11 (2011) 350e357.
[30] C. Tiseanu, B. Cojocaru, V.I. Parvulescu, M. Sanchez-Dominguez, P.A. Primus, M. Boutonnet, Order and disorder effects in nano-ZrO_2 investigated by micro-Raman and spectrally and temporarily resolved photoluminescence, Phys. Chem. Chem. Phys. 14 (2012) 12970e12981.
[31] K. Utt, M. Part, T. Tatte,€ V. Kiisk, M.G. Brik, A.A. Chaykin, I. Sildos, Spectroscopic properties of Eu-doped Y-stabilized ZrO_2 microtubes, J. Lumin. 152 (2014) 125e128.
[32] M. Lee, J. Tang, R.M. Hochstrasser, Fluorescence lifetime distribution of single molecules undergoing Forster€ energy transfer, Chem. Phys. Lett. 344 (2001) 501e508.
[33] J.C. Ray, A.B. Panda, C.R. Saha, P. Pramanik, Synthesis of niobium(V)-stabilized tetragonal zirconia nanocrystalline powders, J. Am. Ceram. Soc. 86 (2003) 514e516.
[34] L.G. Van Uitert, L.F. Johnson, Energy transfer between rare-earth ions, J. Chem. Phys. 44 (1966) 3514e3522.
[35] S. Lange, V. Kiisk, J. Aarik, M. Kirm, I. Sildos, Luminescence of ZrO_2 and HfO_2 thin films implanted with Eu and Er ions, Phys. Status Solidi C 4 (2007) 938e941.
[36] S. Kaneko, T. Morimoto, Y. Ohki, Cause of the appearance of oxygen vacancies in Yttria-stabilized zirconia and its relation to 2.8 eV photoluminescence, Jpn. J. Appl. Phys. 54 (2015), 06GC03.
[37] J.-M. Costantini, F. Beuneu, W.J. Weber, Radiation damage in cubic-stabilized zirconia, J. Nucl. Mater. 440 (2013) 508e514.
[38] D.M. Ramo, J.L. Gavartin, A.L. Shluger, G. Bersuker, Spectroscopic properties of oxygen vacancies in monoclinic HfO_2 calculated with periodic and embedded cluster density functional theory, Phys. Rev. B 75 (2007) 205336.

Institute of Solid State Physics, University of Latvia as the Center of Excellence has received funding from the European Union's Horizon 2020 Framework Programme H2020-WIDESPREAD-01-2016-2017-TeamingPhase2 under grant agreement No. 739508, project CAMART²